Design of formation control laws for manoeuvred flight

G. Campa, S. Wan, M. R. Napolitano and B. Seanor
Department of Mechanical and Aerospace Engineering
West Virginia University, Morgantown, USA

M. L. Fravolini
Department of Electronic and Information Engineering
Perugia University, Perugia, Italy

ABSTRACT

This paper presents identification, control synthesis and simulation results for an YF-22 aircraft model designed, built, and instrumented at West Virginia University. The ultimate goal of the project is the experimental demonstration of formation flight for a set of 3 of the above models. In the planned flight configuration, a pilot on the ground maintains controls of the leader aircraft while a wingman aircraft is required to maintain a pre-defined position and orientation with respect to the leader. The identification of both a linear model and a nonlinear model of the aircraft from flight data is discussed first. Then, the design of the control scheme is presented and discussed with an emphasis on the amount of information, relative to the leader aircraft, needed by the wingman to maintain formation. Using the developed nonlinear model, the control laws for a maneuvered flight of the formation are then simulated with Simulink® and displayed with the Virtual Reality Toolbox®. Simulation studies have been performed to evaluate the effects of specific parameters and the system robustness to atmospheric turbulence. The conclusions from this analysis have allowed the formulation of specific guidelines for the design of the electronic payload for formation flight.

NOMENCLATURE

BLS	batch least squares
DI	dynamic inversion
SQP	sequential quadratic programming
UAV	unmanned aerial vehicle
UCLA	University of California Los Angeles
WVU	West Virginia University
A_x	forward acceleration in body axis (g)
A_y	lateral acceleration in body axis (g)
A_z	normal acceleration in body axis (g)
b	wingspan (m)
$\bar{c}$	mean Aerodynamic cord (m)
C_D	aerodynamic drag force coefficient
C_L	aerodynamic lift force coefficient
C_Y	aerodynamic lateral force coefficient
C_m	aerodynamic pitching moment coefficient
C_l	aerodynamic rolling moment coefficient
C_n	aerodynamic yawing moment coefficient
f	state evolution function of a dynamic system
f	forward clearance error between leader and wingman's aircraft
f_c	predefined forward clearance between leader and wingman's aircraft
F_A	aerodynamic forces acting on the aircraft (N)
g	output function of a dynamic system
g	gravitational acceleration (g)
G	vector of geometric parameters and inertia coefficients
G_a	actuator dynamics transfer function
G_{TT}	throttle to thrust transfer function
G_{vt}	throttle to velocity transfer function
G_{VT}	thrust to velocity transfer function
h	lateral clearance error between leader and wingman's aircraft
h_c	predefined vertical clearance between leader and wingman's aircraft
H	altitude
I	inertia coefficient (kgm²)
K	control gain
l	lateral clearance error between leader and wingman's aircraft
l_c	predefined lateral clearance between leader and wingman's aircraft
m	mass (Kg)
M_A	aerodynamic moments acting on the aircraft (N*m)
p	roll rate (deg/s)
q	pitch rate (deg/s)
$\bar{q}$	dynamic pressure (psi)
r	yaw rate (deg/s)
S	wing platform area (m²)
T	thrust (N)
u	input vector of a dynamic system
V	speed
x	state vector of a dynamic system
x	Longitudinal axes of a reference frame/position of an object along the x axes.

Paper No. 2836. Manuscript received 31 March 2003, accepted 27 November 2003.

https://doi.org/10.1017/S0001924000151577 Published online by Cambridge University Press

y output vector of a dynamic system
y lateral axes of a reference frame/position of an object along the y axes.
z vertical axes of a reference frame/position of an object along the z axes.

α attack angle (deg)
β sideslip angle (deg)
δ vector containing δ_E, δ_A, δ_R, δ_T
δ_E elevators deflection (deg)
δ_A ailerons deflection (deg)
δ_R rudders deflection (deg)
δ_T throttle input (μV)
Δ difference
φ roll angle (deg)
θ pitch angle (deg)
Ω vertical component of the trajectory-induced angular velocity

$_0$ trimmed condition
$_d$ desired value
$_L$ leader
$_W$ wingman
$_x$ projection along the longitudinal axis
$_{xy}$ projection along the horizontal plane
$_y$ projection along the lateral axis
$_z$ projection along the vertical axis

1.0 INTRODUCTION

Autonomous formation flight is an important research area in the aerospace community. The aerodynamic benefits of formation flight, and in particular close formation flight, have been well documented[1-3]. The control of the leader-wingman formation has been investigated extensively[4,5], leading to the introduction of different types of compensation-type controllers[4-6].

In Ref. 7 a formation flight control scheme was proposed based on the concept of Formation Geometry Center, also known as the Formation Virtual Leader. Reference 8 describes the application of an 'extremum seeking' algorithm to the formation control problem. More complex control laws based upon Linear Quadratic Regulator and Dynamic Inversion (DI) approaches have also been proposed[9-11]. Particularly, in Ref. 10, the DI-based approach has been augmented with neural networks to cancel the dynamic inversion error, following the methodology outlined in Ref. 12.

A variety of research efforts are currently on-going within the activities of the AFF (Autonomous Formation Flight) program at NASA Dryden[13-15]. The Boeing Company, UCLA, and NASA Ames are also involved in the AFF program. References 13-15 — from the AFF program — describe in detail the current efforts in modeling the aerodynamic interference between the different aircraft within the formation. Of particular interest from a control point of view are the efforts described in Refs 16,17 where baseline constant-gain compensation-type control laws to maintain formation geometry are compared through simulation studies with adaptive control techniques to achieve robustness to un-modeled portions of the aerodynamic interference. Finally Ref. 18 presents initial flight results of the testing of a formation flight autopilot designed with a compensation-type approach.

This paper presents design results of the formation control laws to be implemented on a set of three YF-22 aircraft models that are designed, built, and instrumented at West Virginia University (WVU). One of the three WVU YF-22 models is shown in Figure 1. The model features an 8ft fuselage length with a 6·5ft wingspan for an approximate take-off weight of 48lb, including a 12lbs electronic payload consisting on a PC-104 flight computer, a complete set of sensors, a GPS receiver and a set of RF modems used for data transmission. The aircraft models are currently undergoing individual flight-tests with flight-testing of the formation control laws to be performed in 2003-2004. Due to the limitations on the flight range, the WVU YF-22 models will be expected to perform fairly tight maneuvers at high Euler angles and moderately high angular rates. Therefore, a specific issue is the design of a control scheme allowing for formation control under these flight conditions. Another objective is to design a formation control scheme with a limited amount of information exchange (between leader and wingman) needed to maintain the predefined formation geometry.



Figure 1. WVU YF-22 aircraft model.

The paper is organised as follows. The second section describes the identification of a linear and nonlinear single aircraft model from collected flight data. The third section outlines the geometric characteristics of the formation. The fourth section outlines the design of the formation control laws. The final sections will present the simulation and visualisation environment, together with the main results.

2.0 SYSTEM IDENTIFICATION AND MODELING OF THE WVU YF-22

The availability of an accurate mathematical model of the aircraft system for designing the formation control laws was a fundamental issue.

2.1 Linear Identification: theoretical background and available tools

The problem of identifying a linear model of a system from its measured input and output data is well known[19,20,21]. In the particular case in which all the states — and their time derivatives for the continuous time system identification — are available for measurement, the system identification problem reduces itself to a multiple linear regression problem[21,22]. In these cases, the problem consists essentially in solving an over-determined linear system in the least squares sense (leading to the well known 'Batch Least Squares' (BLS) method), which is simply solved by pseudo-inverting a large matrix. This methodology can be also easily adapted to the case when some elements of the solution are fixed a-priori.

2.2 Flight data measurement and recording

Flight data for several maneuvers were collected for parameter identification purposes using the following on-board instrumentation.:

https://doi.org/10.1017/S0001924000151577 Published online by Cambridge University Press

- Absolute and differential pressure sensors: (SenSym ASCX15AN and SenSym ASCX01DN) to measure H and V (altitude and speed).
- Inertial measurement unit (Crossbow DMU-VGX) to measure A_x, A_y, A_z, p, q, r, φ, θ, (accelerations, roll pitch and yaw rates, roll and pitch angles).
- Custom designed nose probe to measure α and β (attack and sideslip angles).
- Potentiometers on the control surfaces to measure δ_E, δ_A, δ_R (elevators, ailerons and rudders deflections).

During the flight, the PC-104 based on-board computer collects in real time (at a rate of 100Hz) all of the above signals using the integrated data acquisition card (Diamond MM 32), and stores them on a flash-card for post-flight downloading. A set of flight data was used for the actual parameter estimation process, while a second set of data was used for validation purposes.

2.3 Linear identification process and resulting linear model

The model identification was performed with a 3-step process. First, the flight data time histories were inputted to a Simulink scheme providing smoothing and rearrangement of the signals. Next, a batch Matlab file performed a number of identification algorithms either based on the Matlab System Identification Toolbox or on general BLS methods. Each method gave as a result a linear (affine) system.

The last step of the model identification process was the validation of the linear models. Essentially, the linear models were presented with the time histories of the control surface deflections from the validation flight data, and their outputs were compared with the corresponding signals from the actual flight data. The model produced by the BLS method provided the best fit with the flight data. Following the identification study, the estimated (short period) linear lateral-directional model is given by:

$$\begin{bmatrix}\dot{\beta}\\ \dot{p}\\ \dot{r}\end{bmatrix}=\begin{bmatrix}0.4299 & 0.0938 & -1.0300\\ -67.3341 & -7.9485 & 5.6402\\ 20.5333 & -0.6553 & -1.9955\end{bmatrix}\begin{bmatrix}\beta\\ p\\ r\end{bmatrix}+\begin{bmatrix}0.2724 & -0.7713\\ -101.8446 & 33.4738\\ -6.2609 & -24.3627\end{bmatrix}\begin{bmatrix}\delta_A\\ \delta_R\end{bmatrix} \quad \ldots(1)$$

The estimated (short period) longitudinal model is given by:

$$\begin{bmatrix}\dot{\alpha}\\ \dot{q}\end{bmatrix}=\begin{bmatrix}-4.1172 & 0.7781\\ -33.8836 & -3.5729\end{bmatrix}\begin{bmatrix}\alpha\\ q\end{bmatrix}+\begin{bmatrix}0.5435\\ -39.0847\end{bmatrix}\delta_E \quad \ldots(2)$$

More details on the different identification approaches leading to the determination of the mathematical model of the WVU YF-22 models are available in Ref. 23.

2.4 Nonlinear identification process and resulting nonlinear model

The identification of the mathematical model of a nonlinear system is a more challenging issue[19,24]. Most of the nonlinear identification efforts rely on both good physical insight[19] and some form of optimisation algorithm like Steepest descent or Newton-Raphson[24]. The general nonlinear model of an aircraft system can be expressed as[25]:

$$\begin{aligned}\dot{x} &= f(x,\delta,G,F_A(x,\delta),M_A(x,\delta));\\ y &= g(x,\delta,G,F_A(x,\delta),M_A(x,\delta));\end{aligned} \quad \ldots(3)$$

where x is the state vector (linear and angular positions and velocity), y is the output vector (linear and angular accelerations), δ is the input vector (surface deflections), $\mathbf{G}$ is a vector of geometric parameters and inertia coefficients, F_A and M_A are aerodynamic forces and moments acting on the aircraft; finally, f and g are the known analytic functions that express the dynamics and kinematics of a rigid body. The aerodynamic forces and moments are expressed using the aerodynamic coefficients C_D, C_Y, C_L, C_l, C_m, C_n:

$$F_A=\bar{q}S\begin{bmatrix}C_D(x,\delta)\\ C_Y(x,\delta)\\ C_L(x,\delta)\end{bmatrix}, M_A=\bar{q}S\begin{bmatrix}bC_l(x,\delta)\\ \bar{c}C_m(x,\delta)\\ bC_n(x,\delta)\end{bmatrix} \quad \ldots(4)$$

where S is the wing platform area, $\bar{q}$ the dynamic pressure, b the wingspan, and $\bar{c}$ the mean aerodynamic chord. The aerodynamic coefficients are often approximated by affine functions in x and δ; for example, for the lift coefficient:

$$C_L(x,\delta)=c_{L0}+c_{L\alpha}\alpha+c_{Lq}q+c_{L\delta_e}\delta_e \quad \ldots(5)$$

where, c_{L0} and the other three coefficients are usually called the 'derivatives' of C_L.

When the above approximations are considered satisfactory, the nonlinear aircraft model is completely determined by its aerodynamic derivatives as well as by its inertial and geometric coefficients (which can typically be evaluated experimentally). In this effort, the inertial and geometric characteristics of the WVU YF-22 model were determined with an experimental set-up; thus, the remaining critical issue was the determination of the aerodynamic derivatives.

Formulas to calculate the entries of the matrices of the linear model in Equations (1) and (2) from the values of the aerodynamic derivatives and geometric-inertial parameters are well known[25]. By inverting such formulas, an initial value for all the main aircraft aerodynamic derivatives was then calculated from the matrices in Equations (1) and (2) together with the measured geometric and inertial parameters.

Next, a parameter optimisation routine based on routines available with the Matlab Optimization Toolbox® was set up. Specifically, a Matlab routine was written such that it could take as an input the aerodynamic derivatives to be estimated, perform a simulation with the nonlinear model resulting from those derivatives, compare the outputs with the real data, and return the difference (to be minimised) to the caller function. The *"fmincon"* function — which features the constrained optimisation of a multivariable function using a Sequential Quadratic Programming (SQP) technique[27] — was then used to find the set of aerodynamic derivatives providing the best fit with the flight data, starting from the initial set of aerodynamics derivatives calculated from the linear models. The importance of starting the minimization from a set of already accurate derivatives should be emphasised; in fact, this last optimisation can be considered a refinement of the parameters.

A final validation of the nonlinear model was then conducted using the validation flight data set, similarly to what was done for the linear model. As shown in Fig. 2, the agreement between simulated and real data is substantial. The resulting aircraft nonlinear model is given by:

Geometric and inertial data (60% fuel load):

$\bar{c}$ = 0·7649m, b = 1·9622m, S = 1·3682m²,
I_{xx} = 1·6073kg m², I_{yy} = 7·5085kg m²,
I_{zz} = 7·1865kg m² I_{xz} = –0·3075kg m²
mass = 20·6384kg, T(engine thrust force) = 54·6175N

Longitudinal aerodynamic derivatives:

C_{D0} = 0·0085, C_{Da} = 0·50794, C_{Dq} = 0,
$C_{D\delta E}$ = –0·03,
C_{L0} = –0·0491, C_{La} = 3·258, C_{Lq} = 0,
$C_{L\delta E}$ = 0·189,
C_{m0} = 0·0226, C_{ma} = –0·47, C_{mq} = –3·449,
$C_{m\delta E}$ = –0·364,

https://doi.org/10.1017/S0001924000151577 Published online by Cambridge University Press

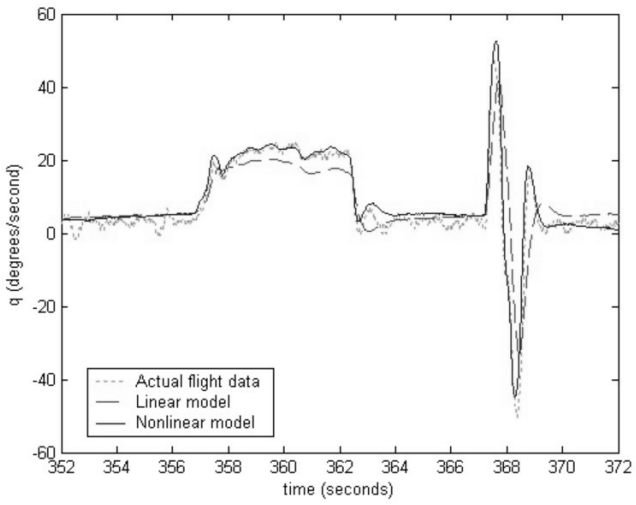


Figure 2. Linear and nonlinear model prediction versus real flight data.

Lateral-directional aerodynamic derivatives:

C_{Y0} = 0·015, C_{Yb} = 0·2725, C_{Yp} = 1·2151, C_{Yr} = –1·1618, $C_{Y\delta A}$ = 0·18363, $C_{Y\delta R}$ = –0·4591,
C_{l0} = –0·001, C_{lb} = –0·037, C_{lp} = –0·2134, C_{lr} = 0·11474, $C_{l\delta A}$ = –0·055929, $C_{l\delta R}$ = 0·0141,
C_{n0} = 0, C_{nb} = 0·0361, C_{np} = –0·151, C_{nr} = –0·19583, $C_{n\delta A}$ = –0·0358, $C_{n\delta R}$ = –0·0554,

The above parameters uniquely define the nonlinear aircraft model in Equation (3), and could easily be used within standard rigid body 6DOF aircraft dynamics simulation tools such as FDC or Airlib[26].

As a final note, it should be emphasised that the wake effects from the leader on the wingman have not been modeled and are assumed to be negligible in a preliminary analysis due to the limited size and airspeed of the models. The net effects of modeling the aerodynamic interference between the different aircraft in the formation can be modeled as 'Δ' terms to the above aerodynamic coefficients. A more refined model could include the wake effects as described in Refs 13-15. An additional approach based on 'Multiple Shoe Vortex Theory' for modelling the wake effects is outlined in Ref. 28.

3.0 Geometry of the formation control problem

The main purpose of this research effort is to design, simulate, and test a formation controller that allows the wingman aircraft to follow the leader — remotely flown by a pilot with a radio control – at pre-defined vertical, forward, and lateral distances during the flight phases when formation flight is engaged. From a geometric point of view the formation flight control problem can be naturally decomposed into two independent problems: a level plane tracking problem and a vertical plane tracking problem, to be described in the following sections.

3.1 Level plane formation definition

Figure 3 shows the level plane formation geometry. All trajectory measurements, i.e., leader/wingman position and velocity, are defined with respect to a pre-defined Earth-Fixed Reference *x–o–y* plane and are measured by the on-board GPSs. The pre-defined formation geometric parameters are the forward clearance f_c and lateral clearance l_c. The forward distance error f and lateral distance error l

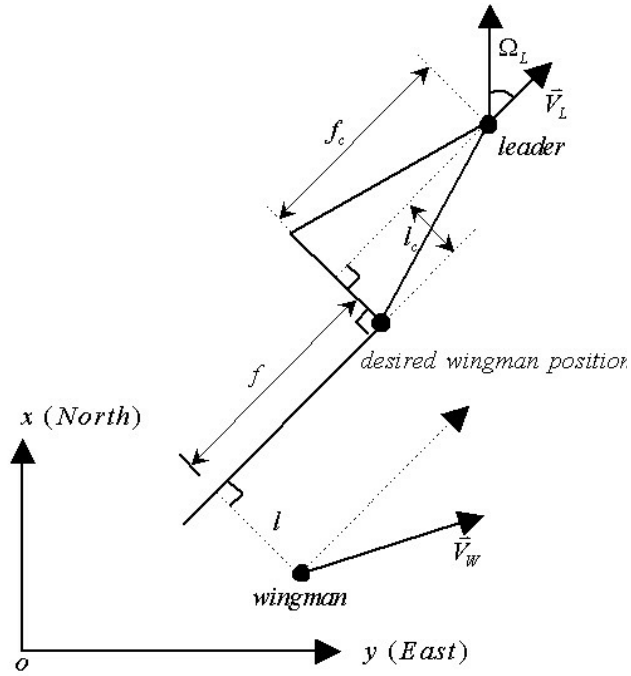


Figure 3. Level plane formation geometry.

can be calculated from the trajectory measurements and formation geometric parameters using the relationships:

$$l = \frac{V_{Ly}(x_L - x_W) - V_{Lx}(y_L - y_W)}{V_{Lxy}} - l_c \quad \ldots (6)$$

$$f = \frac{V_{Ly}(y_L - y_W) + V_{Lx}(x_L - x_W)}{V_{Lxy}} - f_c \quad \ldots (7)$$

where $V_{Lxy} = \sqrt{V_{Lx}^2 + V_{Ly}^2}$ is the projection of the leader's velocity onto the *x–y* plane. Accordingly, the relative forward and lateral speed of the wingman are defined as the time derivatives of the forward and lateral distance respectively and are needed for formation control purposes which can be calculated as:

$$\dot{l} = \frac{V_{Lx}V_{Wy} - V_{Ly}V_{Wx}}{V_{Lxy}} + (f + f_c)\dot{\Omega}_L \quad \ldots (8)$$

$$\dot{f} = V_{Lxy} - \frac{V_{Lx}V_{Wx} + V_{Ly}V_{Wy}}{V_{Lxy}} - (l + l_c)\dot{\Omega}_L \quad \ldots (9)$$

There are two methods to obtain the trajectory-induced angular velocity in the *x–y* plane (around the vertical axis) $\dot{\Omega}_L$. The first method is based on the use of the velocity vector (V_{Lx}, V_{Ly}) , as measured by the on-board GPS, and its time derivative:

$$\dot{\Omega}_L = \frac{\dot{V}_{Ly}V_{Lx} - V_{Ly}\dot{V}_{Lx}}{V_{Lx}^2 + V_{Ly}^2} \quad \ldots (10)$$

A problem with this approach is that the numerical derivative of the velocity vector is sensitive to measurement noise. A second approach is based on using additional measurements from the leader

https://doi.org/10.1017/S0001924000151577 Published online by Cambridge University Press

aircraft along with the following kinematic relation (assuming $\dot{\beta}_L = 0$):

$$\dot{\Omega}_L \cong \dot{\psi}_L = (q_L \mathrm{Sin}\,\phi_L + r_L \mathrm{Cos}\,\phi_L)/\mathrm{Cos}\,\theta_L \quad \ldots (11)$$

This second approach not only requires the vertical gyro (to measure bank angle ϕ_L and pitch angle θ_L) but also the angular rate gyros (to measure pitch rate q_L and yaw rate r_L) to be installed on the leader aircraft.

The level plane formation control problem has been further divided into a lateral distance control problem and a forward distance control problem, to be addressed in Sections 4.1-4.4.

3.2 Vertical plane formation definition

At nominal conditions, the leader and wingman aircraft are separated by a vertical clearance h_c. The vertical distance error h, can then be calculated by:

$$h = z_L - z_W - h_c \quad \ldots (12)$$

while its time derivative is given by:

$$\dot{h} = V_{Lz} - V_{Wz} \quad \ldots (13)$$

The 'vertical control problem' is reduced to the issue of maintaining the vertical clearance h_c.

Based on the above subdivision of the formation geometry, the design of the control laws are separated into three channels to control respectively the lateral, forward, and vertical distance. The resulting design is outlined in Sections 4.5 and 4.6.

4.0 DESIGN OF THE FORMATION CONTROL LAWS

During the formation flight testing, all aircrafts will be individually flown for take-off and landing; the formation will be engaged when all aircraft have reached a certain meeting point within the flight range. A specific constraint for this project is that the aircraft need to remain within a visual range. This, in turn, implies that frequent tight maneuvers will have to be performed. In conventional formation control schemes[6], only the relative position and the velocity vector of the wingman with respect to the leader are required by the 'formation-autopilot' of the wingman to maintain the desired formation. The use of this amount of information has shown to be sufficient for formation control with mild maneuvers by the leader. However, under substantial maneuvering conditions, additional aircraft variables from the leader, such as Euler angles, were found to be necessary for the wingman to maintain the formation geometry.

The formation control problem can be classified as a 'target-tracking' problem as opposed to a more conventional 'trajectory-following' problem. In the latter case the trajectory is typically pre-defined and stored within the on-board computer while in the former the trajectory to be followed by the controlled aircraft (i.e. the wingman) is 'dynamically produced' by target (i.e. the leader aircraft). Ideally, to achieve the best trajectory tracking performance, the formation flight control laws, — that is, the wingman flight control laws — should be based on a 'full information' tracking strategy. This concept can be expressed as:

Wingman's control inputs = Leader's control inputs + State error feedback . . . (14)

where the control inputs include deflections for the throttle, elevator, aileron and rudder, while state error feedback consists of 'internal' state variable errors (such as errors in angular rate and Euler angles) and 'trajectory' state variable errors (such as forward distance, lateral distance, and vertical distance) between the leader and wingman.

The rationale behind this approach is the fact that if the wingman was flying at the same position as the leader, a perfect asymptotic tracking (in position and attitude) could be achieved through a state error feedback, since the leader and wingman aircraft would share the same dynamics (assuming same type of aircraft) and the same control inputs. In other words, the leader acts as a reference system for the wingman, so the state feedback control measures the differences between the leader (reference) state and the wingman state, and provides corrections to the wingman control inputs in order to correct these differences. In reality, the *desired* wingman position is shifted with respect to the leader's position; therefore, extra compensation might be needed to account for the difference in the trajectory variables between the leader and the (ideal) wingman.

It should be noted that in this 'full information' approach all the leader's states and control inputs are needed to calculate the wingman control inputs; therefore, a high communication bandwidth between the leader and wingman is required. An additional goal was to formulate a criteria for limiting the amount of data to be exchanged from leader and wingman aircraft while maintaining the geometry of the formation. This issue has direct implications on the required performance — and, therefore, the cost — of commercially available RF modems. Therefore only a few of the leader outputs and states are actually used to calculate the wingman's control inputs, in lieu of the 'full information' approach outlined in Equation (14).

4.1 Lateral distance control

The objective of the lateral distance control is to minimize the lateral distance error l. The basic physical principle of the lateral distance control can be expressed by the following logic:
aileron → roll rate → bank angle → lateral speed → lateral distance

In addition, the function of the rudder command is to augment the lateral-directional stability, by increasing the Dutch Roll damping. Since bank angle rate changes are substantially higher than rate changes in the lateral position, the lateral dynamics exhibit a typical two-time-scale feature. Therefore, the design of the control system can be decomposed into two successive phases, that is, the design of an inner loop controlling the bank angle and augmenting the lateral-directional stability, and the design of an outer loop which tries to maintain a desired lateral clearance with respect to the leader.

The resulting linear control law is given below and shown in Fig. 4, where the subscripts L and W indicate respectively the wingman and leader aircraft.

Inner loop control law:

$$\delta_{AW} = \delta_{AL} + K_p p_W + K_\phi(\phi_W - \phi_d) \quad \ldots (15)$$

$$\delta_{RW} = \delta_{RL} + K_r r_W \quad \ldots (16)$$

https://doi.org/10.1017/S0001924000151577 Published online by Cambridge University Press

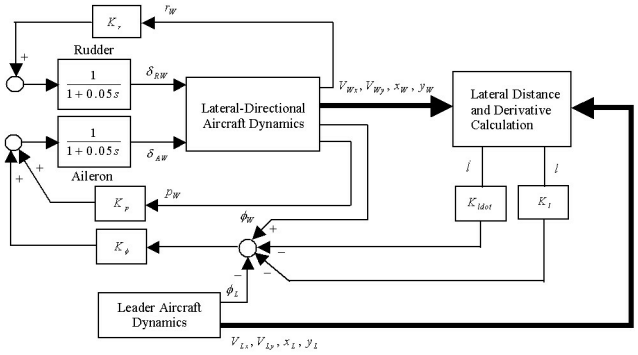


Figure 4. Lateral control law.

Outer loop control law:

$$\phi_d = \phi_L + K_{\dot{l}}\dot{l} + K_l l \qquad \ldots (17)$$

4.2 Lateral-directional model and determination of the controller parameters

The basic lateral-directional linear model of the aircraft is shown in Equation (1). The actuators dynamics are modeled using the following 1st order transfer function:

$$G_a(s) = \frac{1}{1+0{\cdot}05s} \qquad \ldots (18)$$

As discussed in the previous section, the determination of the parameters of the controller is divided into two phases, that is, inner loop and outer loop design. Given the variables involved in Equations (15), (16) and (17), the inner loop controller can be designed based on the aircraft lateral-directional linear model, but the outer loop design requires a suitable kinematic reference model. Such a model can be obtained by considering the aircraft performing a steady state coordinated turn where the lift force balance and centrifugal force balance equations apply. This leads to the following expression:

$$\dot{\Omega}_W = \frac{g}{V_{Wxy}} \mathrm{Tan}\,\phi_W \qquad \ldots (19)$$

Additionally, by assuming a straight and level flight condition of the leader and identical speed for the wingman and the leader, it results that $\Delta\dot{\Omega} = \dot{\Omega}_W$ while Equation (8) takes on the following simple form:

$$\dot{l} = V_{Wxy}\mathrm{Sin}(\Delta\Omega) \qquad \ldots (20)$$

where $\Delta\Omega = \Omega_W - \Omega_L$ .The linearisation of the above two equations (around the standard level-straight flight condition) of the wingman provides the following model of the trajectory dynamics:

$$\begin{cases} \Delta\dot{\Omega} = \dfrac{g}{V_{Wxy}}\phi_W \\ \dot{l} = V_{Wxy}\Delta\Omega \end{cases} \qquad \ldots (21)$$

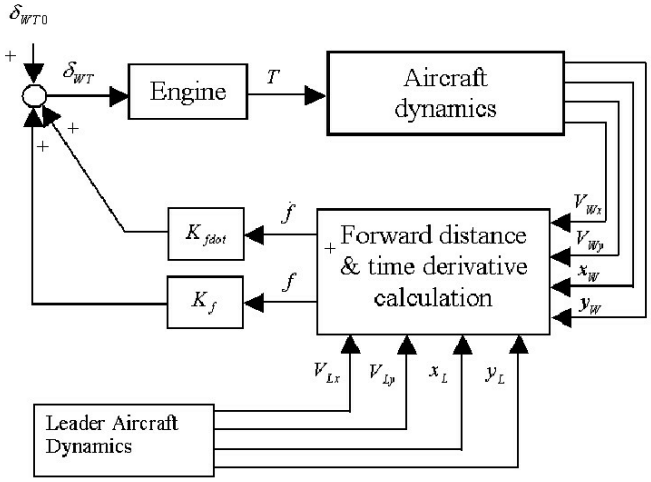


Figure 5 Forward control law.

Thus, the full linear model for lateral distance controller design is the combination of Equations (1), (18), and (21). Classic root-locus based compensation design tools can then be applied to the model for evaluating the controller gains[26]. The basic design specification is to assign the damping ratio of the dominant poles a value around 0·7. The resulting values for the parameters of the different control laws are given by:

$$\begin{aligned} &K_r = 0{\cdot}16, \quad K_p = 0{\cdot}04, \quad K_\phi = 0{\cdot}35 \\ &K_l = 0{\cdot}29, \quad K_{\dot{l}} = 1{\cdot}43 \end{aligned} \qquad \ldots (22)$$

4.3 Forward distance control

The objective of the forward distance control is to minimise the forward distance error *f*. This task can only be accomplished through the use of the throttle control channel. In fact, by increasing/decreasing the throttle, the thrust of the engine and therefore the speed of the aircraft is increased/decreased. This, in turn, allows control of the forward distance between the leader and wingman. The basic physical principle of the forward distance control can be expressed by the following logic:

throttle → *thrust* → *forward speed* → *forward distance*

The forward distance control law, shown in Fig. 5, is given by:

$$\delta_{TW} = \delta_{TL} + K_{\dot{f}}\dot{f} + K_f f \qquad \ldots (23)$$

4.4 Forward model and determination of the controller parameters

The cascade of two first order linear models can approximate the forward dynamics. The 1st model represents the engine response in terms of throttle to thrust; this model has been obtained through an experimental analysis of the performance of the jet engines installed on the WVU YF-22 aircraft; a 2nd model represents the airspeed response in terms of thrust to airspeed, which is approximately derived from the knowledge of nominal thrust, airspeed, mass, and the assumption that the change of aerodynamic drag is in proportional to the change of airspeed.

The following equation represents the resulting complete transfer function of throttle to airspeed:

https://doi.org/10.1017/S0001924000151577 Published online by Cambridge University Press

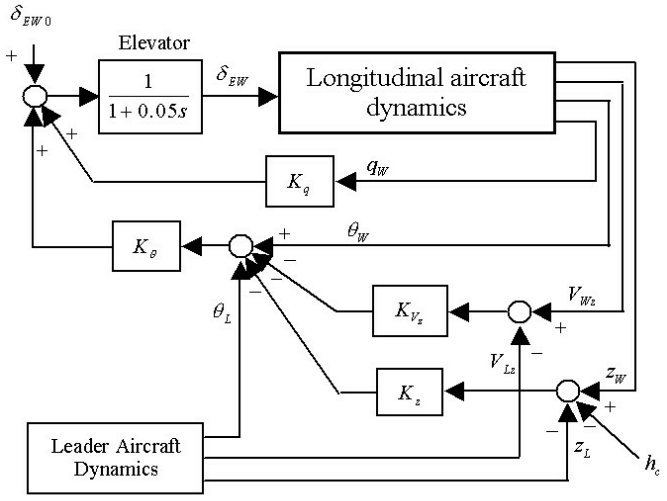


Figure 6. Vertical control law.

$$G_{vt}(s) = G_{VT}(s)\, G_{TT}(s) = \frac{0\cdot 315}{1+6\cdot 5s} \bullet \frac{0\cdot 2}{1+s} \qquad \ldots (24)$$

It should be noted that this model also represents the transfer function from throttle (of wingman) to forward velocity of Equation (9) under the assumed level-straight constant speed flight condition. The parameters of the forward distance controller outlined in Equation (23) were then determined through a root locus-based compensator design. The resulting parameters are:

$$K_f = 0\cdot 4, \quad K_f = 1\cdot 7 \qquad \ldots (25)$$

4.5 Vertical distance control

The objective of the vertical distance control is to minimise the vertical distance error *h*. This task is accomplished through the use of the elevator control channel. The basic physical principle of the vertical distance control can be expressed by the following logic:

elevator → pitch rate → pitch angle → vertical speed → vertical distance

The vertical distance control law is similar to the conventional altitude-hold autopilot with the only difference being that the altitude reference may vary according to the leader's altitude. As with the lateral distance case, the problem exhibits a two time scale structure; thus, the control scheme can be designed using an inner loop controller — which is basically a pitch angle controller — and an outer loop controller providing altitude control.

A linear control law that accomplishes the above scheme is given by the following formulas.

Inner loop control law:

$$\delta_{EW} = \delta_{EL} + K_q q_W + K_\theta(\theta_W - \theta_d) \qquad \ldots (26)$$

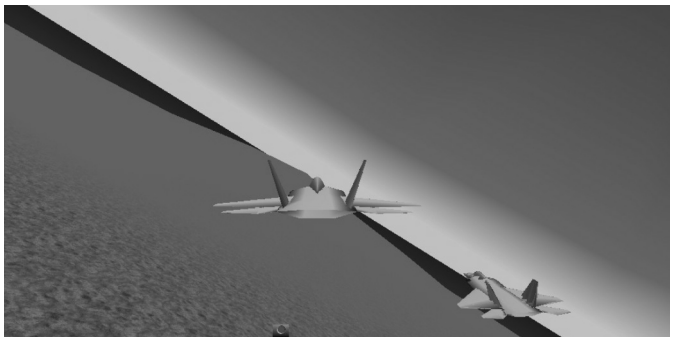


Figure 7. VRT visualisation (behind wingman).

Outer loop control law:

$$\theta_d = \theta_L + K_{\dot z}\dot{\delta z} + K_z \delta z \qquad \ldots (27)$$

The block diagram of the resulting scheme is shown in Fig. 6.

4.6 Vertical model and determination of the controller parameters

The design is based on the linear short period model in Equation (2) in addition to a kinematic model. The linearised kinematic model is given by:

$$\begin{cases} \dot\theta = q \\ \dot h = V_{Wz}\theta \end{cases} \qquad \ldots (28)$$

With a root locus-based design[20] the parameters of the vertical controller are found to be:

$$K_q = 0\cdot 12, \; K_\theta = 0\cdot 50, \; K_z = 5, \; K_{\dot z} = 3 \qquad \ldots (29)$$

5.0 SIMULATION & RESULTS

A Simulink scheme featuring the models of the WVU YF-22 aircrafts and the formation controller was developed and implemented. Given the multi-object nature of the problem, the design of a visualization environment fully integrated with the simulation was considered to be critical. The Virtual Reality Toolbox (VRT) was selected as the visualisation environment since it allows for objects and events of a virtual world (coded in VRML 2.0 or higher[29]) to be driven by signals from Matlab/Simulink. A VRML world including two YF-22 graphical models and a simple landscape which was then implemented and connected with the simulation using the VRT Simulink Blocks. The resulting scenery from a view behind the wingman is shown in Fig. 7.

A preliminary analysis was conducted to assess if deflections of the control surfaces from the leader in Equations (15), (16), (23) and (26) were actually necessary to have desirable tracking performance. This analysis showed that the elimination of these signals from the leader aircraft did not significantly decrease the performance of the control scheme. Consequently, these signals were no longer used (in Equations (23) and (26) two constant trim values were used instead) therefore saving communication bandwidth for flight testing.

Next, two simulation studies were conducted. The purpose of the first study was to assess the need for the bank angle from the leader

https://doi.org/10.1017/S0001924000151577 Published online by Cambridge University Press

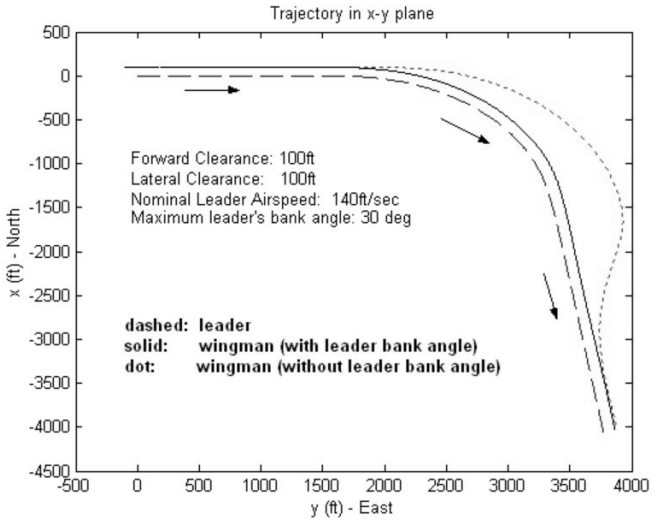


Figure 8. Simulation study #1: trajectories with/without the bank angle from leader aircraft.

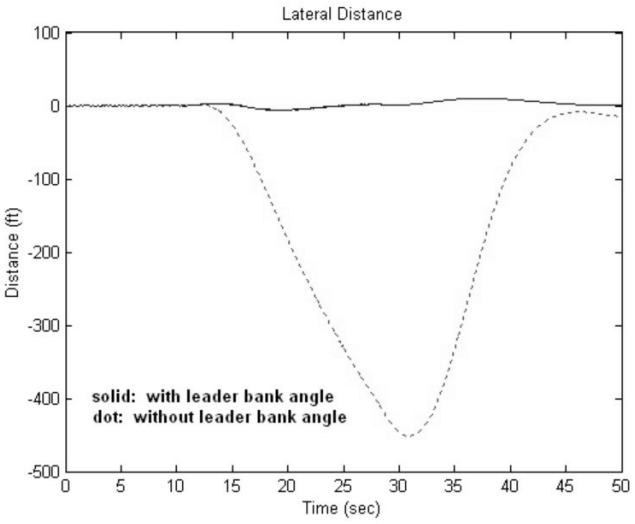


Figure 9. Simulation study #1: lateral distance with/without the bank angle from leader aircraft.

in the wingman control laws in Equation (17). The main results for this study are shown in Figs 8 and 9 where the leader's lateral maneuvering bank angle is about 30°. It can be seen from the simulation that the 'deformation' of the formation in terms of the lateral distance of the wingman from the leader is unacceptably large (as much as 450ft), when the leader's bank angle is not available for formation control purposes. Based on the above considerations, it was decided that the electronic instrumentation of the wingman models will be required to include a three-axis angular rate gyro measuring roll rate p_W , pitch rate q_W and yaw rate r_W, a vertical gyro measuring pitch angle θ_W and bank angle ϕ_W and a GPS receiver measuring the position of the wingman aircraft (with reference to a pre-defined earth-fixed reference) x_W, y_W and z_W, and velocity vector V_{Wx}, V_{Wy} and V_{Wz}. In addition, it was concluded that the pitch angle θ_L and bank angle ϕ_L of the leader aircraft, along with the positions (with reference to a pre-defined earth-fixed reference) x_L, y_L, and z_L, and velocity vector V_{Lx}, V_{Ly} and V_{Lz} are required by the wingman's control system.

The second simulation study was conducted to asses the performance of the formation controller under the following assumptions

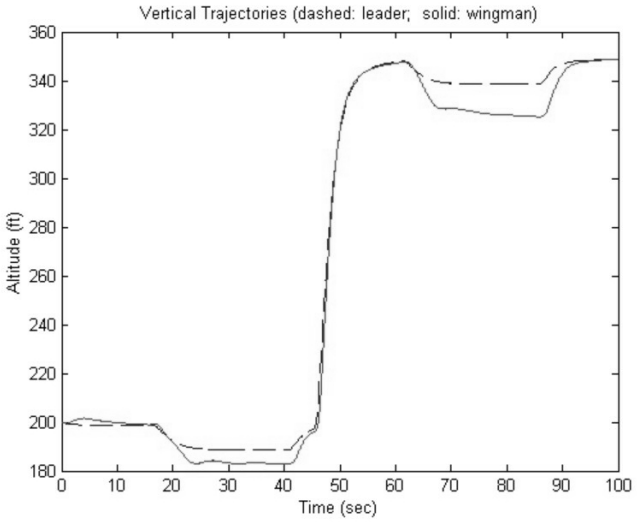


Figure 10. Simulation study #2: trajectories in vertical plane.

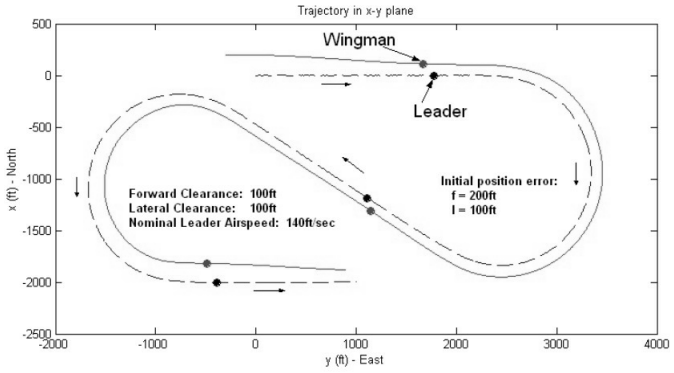


Figure 11. Simulation study #2: trajectories in level plane.

and boundary conditions:

- Leader bank and pitch angles are available to the wingman control system;
- 'S' shape flight trajectory in level plane with a maximum leader bank angle of approx. 50° (as recorded in typical flight tests of the WVU YF-22 models);
- 'Level → climb → level' trajectory in vertical plane;
- Formation geometry: f_c = 100ft; l_c = 100ft, h_c = 0ft (level formation);
- Initial position error: f = 300ft, l = 300ft, h = 0ft;
- Nominal level of atmospheric turbulence.

The simulations were conducted with and without the modeling of wind gusts acting in specific flight segments. Figures 10-12 and Figs 13,14 illustrate the results from this study with and without the wind gust respectively. Table 1 summarizes the performance in terms of maximum tracking errors for different values of the leader maximum bank angle at different configurations (with the wingman flying inside/outside the leader). As expected, a detailed analysis of the results shows that the control scheme provides better performance in terms of maximum forward, lateral and vertical errors with lower leader's bank angles. The large difference between the lateral distance error when the wingman is flying outside/inside the trajectory of the leader is due to the fact that when the wingman is flying inside the leader trajectory the formation control scheme requires a larger bank angle; on the other side, the effectiveness of the lateral distance control is very sensitive to the nonlinear effects due to large increases in the wingman's bank angles.

https://doi.org/10.1017/S0001924000151577 Published online by Cambridge University Press

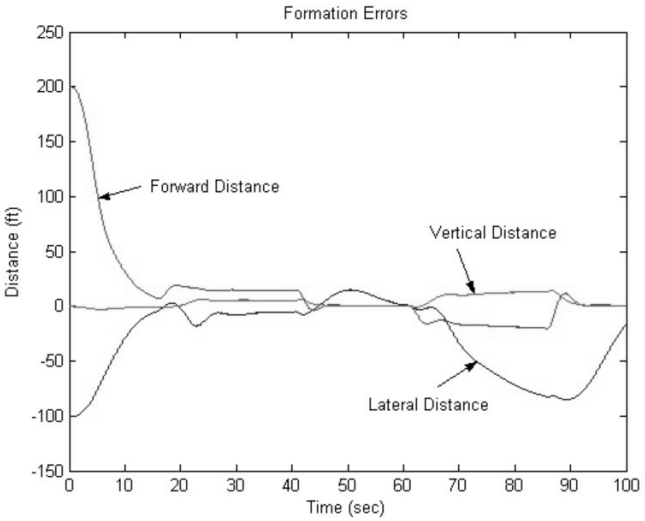


Figure 12. Simulation study #2: formation errors.

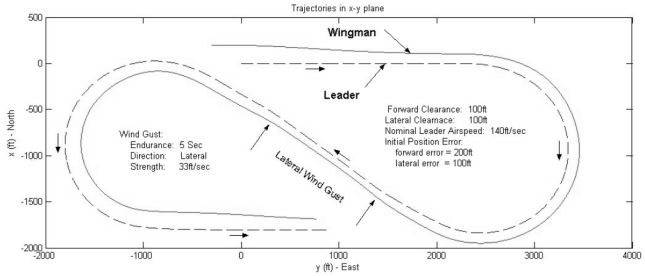


Figure 13. Simulation study #2: trajectories in level plane with lateral wind gusts.

6.0 CONCLUSIONS

This paper presents an approach for the design of linear control laws to maintain specified geometry for a formation of research aircraft models. The design is based on compensation-type controllers for minimising tracking errors along the forward, lateral, and vertical axes. The analysis shows that the availability of the Euler angles from the leader aircraft is critical for the wingman to maintain the assigned formation geometry throughout the maneuvered flight. An additional goal was to evaluate the criteria to limit the necessary data communication between the leader and the wingman. The design has been verified through a set of simulation studies interfacing the aircraft models and the control schemes in Simulink with a VRT environment. The results of the simulation show a desirable performance of the formation control schemes.

ACKNOWLEDGEMENTS

Support for the first four authors is provided through the Air Force Office of Scientific Research Grant F49620-01-1-0373.

Table 1
Tracking errors for different configurations at different bank angles

Leader airspeed: 140ft/sec, Formation geometry: f_c = 100ft, l_c = 100ft, h_c = 0ft

	Maximum lateral distance *l* (ft)		Maximum forward distance *f* (ft)		Maximum vertical distance *h* (ft)	
Wingman's position w.r.t leader	*Outer Turn*	*Inner Turn*	*Outer Turn*	*Inner Turn*	*Outer Turn*	*Inner Turn*
F_L						
20°	7·7	18·5	11·0	11·1	0·6	2·1
25°	9·1	25·8	12·6	12·7	1·1	3·1
30°	10·4	34·5	14·0	14·1	1·9	4·5
35°	11·5	45·5	15·7	15·9	2·8	6·2
40°	12·7	58·7	17·4	18·1	3·9	8·6
45°	14·0	77·7	19·4	21·9	5·4	11·9
50°	16·6	105·9	21·8	27·3	7·2	17·2
55°	20·0	166·2	26·7	37·0	9·5	28·6

REFERENCES

1. BLAKE, W. and MULTHOPP, D. Design, performance, and modeling considerations for close formation flight, Proceedings of the 1999 AIAA GNC Conference, AIAA paper 1999-4343, Portland, OR, August 1999.
2. PACHTER, M., D'AZZO, J.J. and PROUD, A.W. Tight formation flight control, *J Guidance, Control, and Dynamics*, March-April 2001, **24,** (2), pp 246-254.
3. GIULIETTI, F., POLLINI, L. and INNOCENTI, M. Autonomous formation flight, *IEEE Control Systems Magazine*, 2000, **20,** (6), pp 34-44.
4. PROUD, A.W. Close Formation Flight Control, MS Thesis, AFIT/GE/ENG/99M-24, School of Engineering, Air Force Institute of Technology (AU), Wright-Patterson AFB, OH, March 1999.
5. HALL, J.K. Three Dimensional Formation Flight Control, MS Thesis, AFIT/GE/ENG/00M-06, School of Engineering, Air Force Institute of Technology (AU), Wright-Patterson AFB, OH, March 2000.
6. PACHTER, M., D'AZZO, J.J. and DARGAN, J.L. Automatic formation flight control, *J Guidance, Control, and Dynamics,* 1994, **17,** (6), pp 1380-1383.
7. GIULIETTI, F., POLLINI, L. and INNOCENTI, M. Formation flight control: A behavioral approach, Proceedings of the 2001 AIAA GNC Conference, AIAA Paper 2001-4239, Montreal, Canada, August 2001.
8. BINETTI, P., ARIYUR, K.B., KRSTIC, M. and BERNELLI, F. Control of formation flight via extremum seeking, Proceedings of the 2002 America Control Conference, Anchorage, AK, May 2002.
9. SCHUMACHER, C.J. and KUMAR, R. Adaptive control of UAVs in close-coupled formation flight, Proceedings of the 2000 American Control Conference, Chicago, IL, June 2000.
10. SCHUMACHER, C.J. AND SINGH, S.N. Non linear control of multiple UAVs in close-coupled formation flight, Proceedings of the 2000 AIAA GNC Conference, AIAA paper 2000-4373, Denver, CO, August 2000.
11. SINGH, S.N., PACHTER, M., CHANDLER, P., BANDA, S., RASMUSSEN, S. and SCHUMACHER, C.J. Input-output invertibility and sliding mode control for close formation flying of multiple UAVs, Proceedings of the 2000 AIAA GNC Conference, Denver, CO, August 2000.
12. CALISE, A.J. and RYSDYK, R.T. Nonlinear adaptive flight control using neural networks, *IEEE Control Systems Magazine*, 1998, **18**, (6).
13. RAY, R.J., COBLEIGH, B., VACHON, M.J., and ST JOHN, C. Flight test techniques used to evaluate performance benefits during formation flight, Proceedings of the 2002 AIAA GNC Conference, AIAA paper 2002-4492, Monterey, CA, August 2002.
14. HANSEN, J.L. and COBLEIGH, B.R. Induced moment effects of formation flight using two F/A-18 aircraft, Proceedings of the 2002 AIAA GNC Conference, AIAA paper 2002-4489, Monterey, CA, August 2002.
15. VACHON, M.J., RAY, R.J., WALSH, K.R. and ENNIX, K. F/A-18 aircraft performance benefits measured during the autonomous formation flight project, Proceedings of the 2002 AIAA GNC Conference, AIAA paper 2002-4491, Monterey, CA, August 2002.
16. MISOVEC, K. Applied adaptive techniques for F/A-18 formation flight, Proceedings of the 2002 AIAA GNC Conference, AIAA paper 2002-4550, Monterey, CA, August 2002.
17. LAVRETSKY, E. F/A-18 Autonomous formation flight control system design, Proceedings of the 2002 AIAA GNC Conference, AIAA Paper 2002-4757, Monterey, CA, August 2002.
18. HANSON, C.E., RYAN, J., ALLEN, M.J. and JACOBSON, S.R. An overview of flight test results for a formation flight autopilot, Proceedings of the 2002 AIAA GNC Conference, AIAA paper 2002-4755, Monterey, CA, August 2002.

https://doi.org/10.1017/S0001924000151577 Published online by Cambridge University Press

19. LJUNG, L. *System Identification: Theory for the User,* 2nd Ed, PTR Prentice Hall, Upper Saddle River, Englewood Cliffs, NJ, 1999.
20. VAN OVERSCHEE, DE MOOR B. *Subspace Identification for Linear Systems: Theory, Implementation, Applications.* Kluwer Academic Publishers, 1996.
21. STENGEL, R.F. *Optimal control and estimation,* Dover Publication,New York, 1994.
22. DOBSON, A.J. *An Introduction to Generalized Linear Models,* 1990, CRC Press.
23. NAPOLITANO, M.R., West Virginia University, Air Force Office of Scientific Research (AFOSR) Grant F49620-98-1-0136 Final Report, March 2002.
24. MAINE, R.E. and ILIFF, K.W. Identification of dynamic systems: theory and formulation, NASA RF 1168, June 1986.
25. STEVENS, B. and LEWIS, F. *Aircraft Control and Simulation,* John Wiley & Sons, NY, 1992.
26. CAMPA, G, 'Airlib', (February 2003), http://www.mathworks.com/matlabcentral/fileexchange/
27. HOCK, W. and SCHITTOWSKI, K. A Comparative performance evaluation of 27 nonlinear programming codes, *Computing*, 1983, **30**, p 335.
28. GIULIETTI, F., NAPOLITANO, M.R., CAPETTA, R. and INNOCENTI, M. The complete aircraft model within a formation flight, Proceedings of the 2002 AIAA Atmospheric Flight Mechanics Conference, August 2002
29. The VRML Web Repository (December. 2002): http://www.web3d.org/vrml/vrml.htm

https://doi.org/10.1017/S0001924000151577 Published online by Cambridge University Press